Journal of Catalysis **204,** 450–459 (2001)
doi:10.1006/jcat.2001.3394, available online at http://www.idealibrary.com on IDEAL®

Hydrogenation of Citral on Activated Carbon and High-Surface-Area Graphite-Supported Ruthenium Catalysts Modified with Iron

B. Bachiller-Baeza,* A. Guerrero-Ruiz,† P. Wang,* and I. Rodríguez-Ramos*,[1]

*Instituto de Catálisis y Petroleoquímica, C.S.I.C., Campus de Cantoblanco, 28049 Madrid, Spain; and †Departamento Química Inorgánica y Técnica, U.N.E.D., C/Senda del Rey s/n, 28040 Madrid, Spain

Received June 13, 2001; revised August 16, 2001; accepted August 16, 2001; published online October 25, 2001

The hydrogenation of citral has been performed over Ru–Fe catalysts supported on activated carbon and on high-surface-area graphite. It was found that selectivity to unsaturated alcohols is independent of the carbonaceous support used for ruthenium catalysts. The addition of iron enhances selectivity to unsaturated alcohols (geraniol and nerol) in a manner similar for both ruthenium catalysts, becoming maximum for the highest iron loading. Calorimetric experiments give some evidence about alloy formation in ruthenium catalysts promoted with iron. It is inferred that the surface polarity of the alloyed particles promotes the selective hydrogenation of citral toward unsaturated alcohols.

Key Words: **microcalorimetry; citral; hydrogenation; ruthenium catalysts; iron; carbon supports.**

1. INTRODUCTION

The hydrogenation of α,β-unsaturated aldehydes to unsaturated alcohols has been extensively studied in recent years because of the relevance of these compounds to the pharmaceutical and fine chemicals industry (1, 2). Moreover, much work has been done to develop heterogeneous catalysts applicable to these reactions. On one hand, these systems avoid the production of residues and waste obtained in conventional stoichiometric processes. On the other hand, they alleviate the difficulties associated with the separation and recycling of homogeneous catalysts. Moreover, different approaches to designing a proper catalyst have been used to improve the generally low selectivity to the desired alcohol. It is known that the final selectivity of an active metal can be modified by using an adequate support, which interacts with the metal, or by adding a second component as a promoter. Electronic and geometric effects have been suggested as the explanation for the improvement in selectivity to unsaturated alcohols (3–5).

Some work in this line has focused on the study of carbonaceous materials as supports. The gas-phase hydrogenation of crotonaldehyde has been carried out over platinum catalysts supported on activated carbon and carbon blacks (6, 7). It was observed that selectivity to unsaturated alcohol depended on the number of oxygenated surface groups; the greater the number of oxygenated groups, the higher the selectivity. In contrast, the same reaction was studied over graphite-supported platinum and ruthenium catalysts, and it was concluded that the number of oxygenated surface groups did not influence selectivity. But rather, the presence of residual amounts of chloride ions anchored to the surface oxygen groups enhances unsaturated alcohol selectivity (8). In another investigation graphite-supported catalysts were found to be much more selective than charcoal-supported ones in the liquid-phase hydrogenation of cinnamaldehyde to cinnamyl alcohol (9). It was proposed that the selectivity improvement observed was related to the electron donating properties of the graphite, which was interacting with the metal particles located along the edges of the basal planes.

Higher selectivity for unsaturated alcohols might also be arranged by using a second metal component. It is well-known that various metal salts, such as iron, tin, or germanium chlorides, added to the reaction medium have a positive effect on selectivity to the unsaturated alcohol in the hydrogenation of cinnamaldehyde over platinum catalysts (10, 11). Richard *et al*. found volcano-type activity, a selectivity curve, and an optimum molar ratio for Fe/Pt of 0.2 for the hydrogenation of cinnamaldehyde with Pt/C catalysts and $FeCl_2$ as additive (10). They observed the formation of bimetallic particles with electron-deficient iron atoms acting as Lewis adsorption sites for the activation of the C=O bond. Bimetallic catalysts have also been investigated in the hydrogenation of α,β-unsaturated aldehydes (12–18), with tin and iron being the most effective among the promoters. Moreover, mechanical mixtures of Pt–Fe_2O_3 possess bifunctional properties, iron oxide coordinates the aldehyde molecule, and Pt activates the hydrogen (19). However, exhaustive studies on bimetallic catalysts involving Fe as promoter are scarce. Pt–Fe/C catalysts follow a behavior similar to that obtained by adding iron salt to the reaction medium in the hydrogenation of cinnamaldehyde (20).

In this paper we report on a study of the hydrogenation of citral using bimetallic Ru–Fe catalysts supported on two

[1] To whom correspondence should be addressed. Fax: 34-91-5854760. E-mail: irodriguez@icp.csic.es.

0021-9517/01 $35.00

carbon materials. We have examined the influence of the promoter and the effect of a noninteracting or inert support (active carbon) and of an electron donor support (graphite) on the catalysts reactivity. In addition, the possible combination of the two effects is analyzed. Different techniques are applied for the characterization of the catalysts; in particular, the microcalorimetry of CO adsorption is intended to be correlated with the electronic surface properties of the supported metallic clusters.

2. EXPERIMENTAL

2.1. Catalyst Preparation

The supports used in the preparation of the catalysts were an activated carbon (C, ICASA Spain, $S_{BET} = 964\ m^2/g$) and a high-surface-area graphite (H, Lonza, $S_{BET} = 295\ m^2/g$). The activated carbon was treated with inorganic acids (HCl and HF) and then washed with deionized water to remove inorganic impurities. The graphite was treated to clear the surface from oxygen groups under flow of He at 1173 K (21).

Monometallic catalysts were prepared by incipient wetness of the supports with an aqueous solution of $RuNO(NO_3)_3$. Bimetallic ruthenium–iron catalysts were prepared by a coimpregnation method with aqueous solution of $RuNO(NO_3)_3$ and $Fe(NO_3)_3 \cdot 9H_2O$. All solids were dried overnight at 383 K.

2.2. Characterization of Catalysts

Composition of the catalysts was determined by ICP–AES in a Perkin Elmer 3300 PV after dissolution of the catalysts. Metal loading of the monometallic catalysts was also determined by burning away the carbon in air at 1073 K and weighing the residue. The results of elemental analysis and the Fe/Ru atomic ratios are shown in Table 1.

Temperature-programmed reduction (TPR) experiments were performed using a U-shaped quartz reactor. A high-purity mixture of 4% hydrogen in helium was fed into the reactor and the temperature of the sample was increased from room temperature to 873 K at a rate of $8\ K \cdot min^{-1}$ (22). The effluents of the reactor were analyzed in a gas chromatograph provided with a thermal conductivity detector, an automatic sample injection, and a Porapack Q column.

Temperature-programmed desorption (TPD) experiments were performed under vacuum. The apparatus consists of a quartz bulb directly attached to a quadrupole mass spectrometer (Balzers QMG 421-C) (23). The temperature of the sample was increased from 473 to 1023 K at a rate of $10\ K \cdot min^{-1}$.

The samples after reaction were further analyzed by X-ray photoelectron spectroscopy (XPS). The spectra were obtained on a Physical Electronics 5700 spectrometer equipped with a hemispherical multichannel Electronics 80-365B analyzer. The excitation source was the Mg$K\alpha$ line ($h\nu = 1253.6$ eV, 300 W). The binding energies of Fe $2p_{3/2}$ and Ru $3p_{3/2}$ were referenced to the C 1s line at 284.8 eV. X-ray diffraction patterns of the samples used in the reaction were recorded using a Philips PW 1050/81 apparatus using a filtered Cu$K\alpha$ radiation ($\lambda = 0.1538$ nm) and a graphite monochromator.

2.3. Calorimetric Measurements

The heats of CO adsorption at 330 K were measured in a differential heat-flow microcalorimeter of the Tian–Calvet type C80 from Setaram. The adsorption vessels were linked to a Pyrex volumetric apparatus equipped with greaseless stopcocks that permitted the introduction of small pulses of CO (21). The samples were activated in flowing H_2 at 673 K for 2 h, and after outgassing at this temperature for 16 h were cooled down to the adsorption temperature. Then successive doses of CO were sent onto the sample. The equilibrium pressure was measured by means of a Baratron pressure transducer MKS Instrument. The calorimetric and volumetric data were stored and analyzed using microcomputer processing.

2.4. Activity Measurements

The liquid-phase hydrogenation of citral was carried out at atmospheric pressure under H_2 flow in a five-necked

TABLE 1

Catalyst Characterization

Catalyst	% Ru	% Fe	$(Fe/Ru)_{Chem}$	$(Fe/Ru)_{XPS}$	CO adsorption ($\mu mol \cdot g^{-1}$)	CO/Ru + Fe
Ru/C	1.7	—	—	—	130	0.75
RuFe/C	1.5	0.4	0.4	5.1	87	0.43
RuFe2/C	1.4	1.5	2.0	7.8	81	0.20
Fe/C	—	2.1	—	—	23	0.11
Ru/H	1.9	—	—	—	75	0.40
RuFe/H	1.6	0.5	0.5	1.5	62	0.25
RuFe2/H	1.6	1.8	2.1	4.3	43	0.09

reactor fitted with a stirred head (850 rpm), a thermometer, a reflux condenser, gas entry through a glass filter, and a port for reactant introduction and sample extraction. The catalysts were transferred to the reactor, after reduction in the gas phase at 673 K for 2h, using the conventional Schlenk technique to preserve the catalyst from air exposition. The reactor flask containing the solvent (isopropanol) was heated at 333 K in flowing H_2 and citral was injected (citral/Ru molar ratio of 30) through the charging port. The distribution of products was followed by repetitive sampling. The samples were analyzed by gas chromatography using a MFE-20 capillary column and a flame ionization detector.

Preliminary runs carried out at different stirring conditions, loading, and catalyst grain size demonstrated the absence of external and internal mass transfer limitations.

3. RESULTS AND DISCUSSION

3.1. Catalysts Characterization

The TPR profiles obtained for the monometallic and bimetallic Ru–Fe catalysts are shown in Fig. 1A for the catalysts supported on activated carbon, and in Fig. 1B for the catalysts supported on high-surface-area graphite. Both monometallic Ru catalysts displayed a sharp peak, at 510 K for Ru/C and at 490 K for Ru/H, which corresponds to the reduction of the salt precursor to metallic ruthenium (21). The lower reduction temperature for Ru/H indicates that metal reduction is facilitated in this catalyst. On the other hand, Ru/C catalyst presents a well-defined second H_2 consumption peak at higher temperatures, centered at 660 K. This peak is accompanied by CH_4 evolution and thus could be due to a partial carbon gasification process (22). For the Ru/H catalyst the peak is broader, but again the simultaneous evolution of methane in the same range of temperature is observed. The TPR profile for the Fe/C catalyst shows a peak at 690 K, assigned to the reduction of surface Fe^{3+}. This temperature is within the temperature range reported for the reduction of iron supported on different carbon materials (24–26).

The TPR profiles of the bimetallic catalysts are close to that of the Ru unpromoted catalysts. Thus, only one peak, at 510 K for catalysts supported on activated carbon and at 490 K for the catalysts supported on graphite, is observed. The reducibility of surface metal oxides has been described as being affected by the presence of a noble metal and in general the reduction temperature of the oxide becomes lower (25, 27). Also, it has been reported that the close interaction between the two metals could inhibit the reduction of the noble metal (27). The TPR curves show that reduction of Fe is shifted to lower temperatures, and that the two metals are reduced together. This latter fact is deduced from the following. On the one hand, only a single defined peak is observed in the TPR profile at low and medium temperature ranges. This peak coincides with that of ruthenium reduction in monometallic catalysts, the temperature of which is not raised by the presence of the promoter. On the other hand, the amount of hydrogen consumption corresponding to this peak increases with the iron loading,

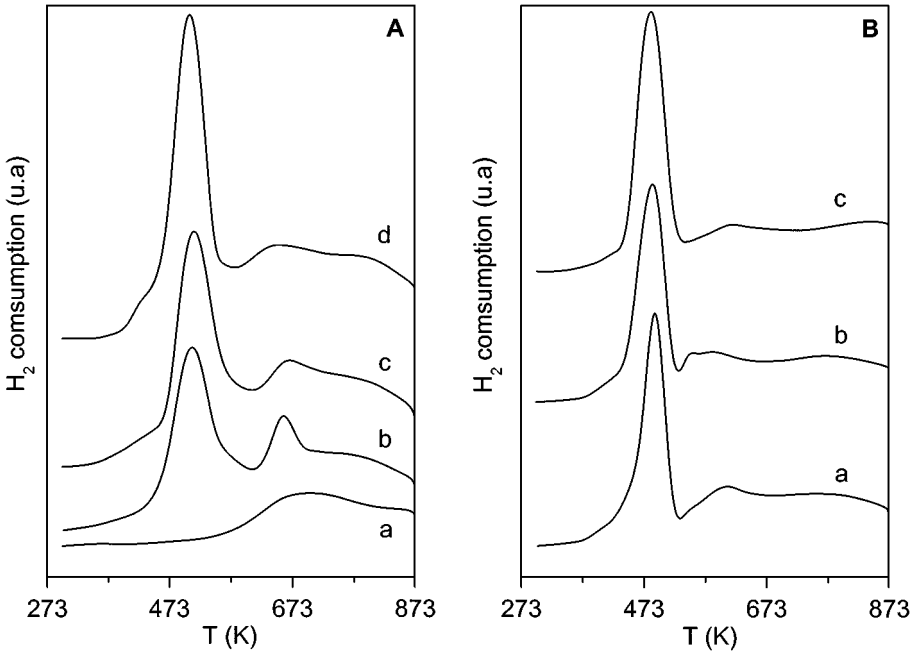

FIG. 1. TPR profiles. (A) Catalysts supported on carbon: (a) Fe/C, (b) Ru/C, (c) RuFe/C, and (d) RuFe2/C. (B) Catalysts supported on graphite: (a) Ru/H, (b) RuFe/H, and (c) RuFe2/H.

suggesting that the peak has to be associated with the reduction of not only Ru but also Fe. Quantitative evaluation of the relative amounts of reduced Ru and particularly Fe is not possible because the reduction reaction involves the reduction of oxides and mainly of undecomposed precursors, and consequently of the NO and NO_3 groups of the molecules. The TPR profiles of bimetallic catalysts show also the peak corresponding to the gasification of the support, but it is less marked than that observed for the Ru monometallic catalysts. These results reveal the reduction in catalytic activity for methane production by the gasification of the carbon support when iron is added as promoter to Ru and can be indicative of specific metal-promoter interactions. Therefore, the TPR patterns of the bimetallic catalysts indicate close proximity of iron and ruthenium.

3.2. *Calorimetric Measurements*

The electronic properties of the surface sites of mono- and bimetallic catalysts were studied using CO adsorption microcalorimetry. The differential heats of CO adsorption on Ru, Fe, and Ru–Fe catalysts with different Fe/Ru atomic ratios, and supported on activated carbon and on graphite, are given in Figs. 2A and 2B, respectively. It can be seen that the initial heats of CO adsorption were very close for the Ru/H (138 kJ/mol) and Ru/C (137 kJ/mol) catalysts. In a first approach these values seem to contradict those of previous studies carried out with Ru catalysts supported on activated carbon and graphite (28, 29). A higher initial heat of CO adsorption was observed on ruthenium/graphite, indicating enhanced electron density in the ruthenium particles caused by electron transfer from the graphite. However, it was also shown that the presence of oxygen groups at the surface of the graphite restrains the metal-support interaction (21). In this work a high-surface-area graphite free of oxygen surface groups was utilized as support. However, the aqueous solution of the ruthenium precursor ($RuNO(NO_3)_3$) used in the preparation of the catalysts has a very high oxidizing character. However, it is known that the active sites present at the edges of the graphitic layers of the carbonaceous materials easily react with an oxidant (HNO_3) and form oxygen functional groups (30). Therefore, it can be inferred that oxygen surface groups were inevitably introduced into the carbonaceous material during the preparation procedure, impeding the electron donor ligand effect of the graphite support over the ruthenium particles supported on it (31). In fact, TPD experiments over the two monometallic ruthenium catalysts show the presence of surface oxygen groups which decompose upon heating in vacuum. The most acidic (carboxyls and lactones) evolve as CO_2 between 473 and 800 K and the less acidic (phenols and carbonyls) evolve as CO above 723 K. Moreover, the activated carbon contains a higher amount of surface oxygen functional groups. This latter fact is expected, given that the proportion of active sites increases as the surface area of the carbon increases.

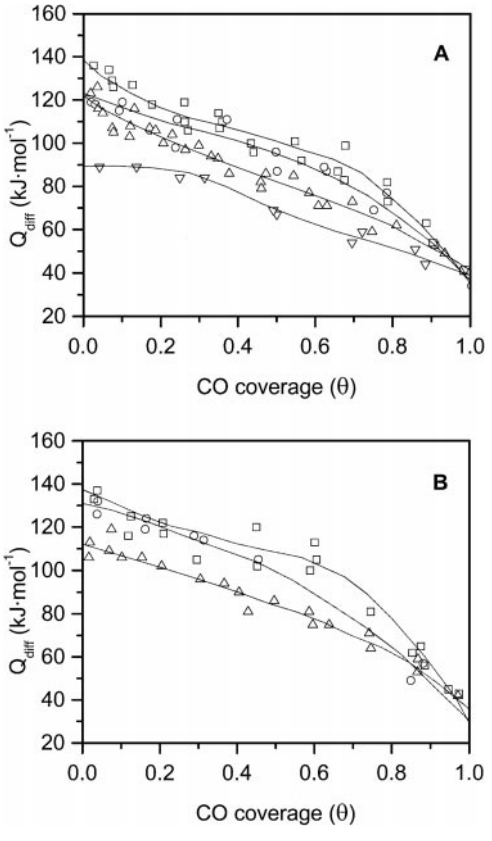

FIG. 2. Differential heats of CO adsorption at 330 K. (A) Catalysts supported on carbon: (□) Ru/C, (○) RuFe/C, (△) RuFe2/C, and (▽) Fe/C. (B) Catalysts supported on graphite: (□) Ru/H, (○) RuFe/H, and (△) RuFe2/H.

Moreover, the calorimetric profiles for the Ru/C and Ru/H catalysts show that the energetic distribution of the CO adsorption sites is very heterogeneous (Fig. 2). The differential heat of CO adsorption on Ru seems to steadily decrease from the start, although in the range of coverage between 0.3 and 0.6 the rate of fall is slower. On the other hand, the Fe/C catalyst shows a plateau at the initial heat of adsorption up to a coverage of approximately 0.2, at which point the heat values slowly fall until physical adsorption is reached. It is worth noting that the initial differential heat of CO adsorption on Fe is lower than on Ru. The formation of subcarbonyls species by the admission of CO onto reduced samples containing Fe^0 crystallites is expected (32, 33). The formation of this type of species explains the lower initial heat of adsorption observed for the iron catalyst. Although few measures of CO chemisorption on Fe have been performed, the initial heat value compares well with the data for CO adsorption on films and with that determined on a Fe supported on MgO catalyst (34, 35). The latter authors found a particle-size dependence in the distribution of CO adsorption heat. In particular, the amount of weakly bound CO (80–90 KJ/mol) increases with increasing dispersion.

The initial heats of adsorption for the Ru–Fe catalysts supported on activated carbon are lower than that for Ru/C, 122 kJ/mol. The two promoted bimetallic catalysts with different Fe/Ru ratios display similar heat-of-adsorption shapes falling between the two monometallic extremes throughout the coverage range (Fig. 2A). Moreover, the increase in the Fe/Ru ratio results in a calorimetric curve approaching that of the iron monometallic catalyst. On the other hand, the addition of Fe to the Ru/C catalyst reduced also the extent of CO adsorption on the surface. The saturation coverages of carbon monoxide on the investigated catalysts are tabulated in Table 1. It can be seen that the saturation extent of carbon monoxide is almost constant with increasing content of iron for catalysts supported on activated carbon. As for the bimetallic catalysts supported on high-surface-area graphite, the initial heats of CO adsorption are lower than that for the monometallic ruthenium, and they decrease with increasing iron content, from 143 to 133 and 112 kJ/mol for 0.5 and 2.1 Fe/Ru ratios, respectively (Fig. 2B). Concerning the saturation coverage, while for activated carbon-supported catalysts the amount of adsorbed CO is constant with increasing Fe loading, for graphite-supported catalysts it decreases with increasing Fe/Ru ratio (Table 1). It can be concluded that the addition of Fe to Ru/C and Ru/H catalysts results in a weakening of the CO bound states and a decrease in the amount of CO adsorbed. Surface analysis of catalysts by XPS shows that the surface of the metal crystallites is enriched in Fe compared to the bulk composition, with the iron enrichment increasing with increasing Fe/Ru ratio (Table 1). This fact agrees well with data reported for carbon-supported and unsupported Ru–Fe alloys (36, 37). This surface-iron enrichment is to be expected in Ru–Fe alloys from the fact that iron has a lower surface energy than does ruthenium (36). Previous Mössbauer spectroscopy results obtained on carbon-supported Ru–Fe catalysts showed the formation mainly of the Ru–Fe alloy and also of a small amount of segregated metallic iron (25).

On the basis of the heat of CO adsorption data presented above, it appears that the surface of the metallic particles in the Ru–Fe catalysts is possibly an alloyed phase. This is inferred from several aspects of the data. First, the differential heat curves of the bimetallic catalysts fall monotonically between the two monometallic extremes. Segregation of the two metals would imply initial ruthenium-like heat, since CO is expected to preferentially adsorb on ruthenium sites at low coverage due to its higher CO adsorption heat. Furthermore, the differential heat would fall off as the iron sites became more important. Second, the total CO uptake is nearly half that expected for a surface composed of two segregated metals. This can be explained by either a decrease in the metal surface area or a change in the CO adsorption stoichiometry on the Ru–Fe alloyed phase. Clear diffraction peaks assigned to Ru, Fe, or RuFe alloy did not appear in the XRD patterns even in the samples with higher iron content. This latter fact implies that the size of the metallic crystallites remains below the size limit of XRD detectability (<4 nm) and therefore they could not be detected. The TPR profiles of the bimetallic catalysts have shown the simultaneous reduction of the two metals, supporting the formation of a Ru–Fe alloy.

3.3. Activity Measurements

The desired products of citral hydrogenation are the unsaturated alcohols geraniol and nerol, which are obtained through hydrogenation of the C=O bond of the two isomers E and Z of citral. However, different products, from the isolated or the conjugated C=C double-bond reduction and successive hydrogenation of the primary products, can be produced as displayed in the reaction scheme (Scheme 1). The reaction of citronellal with the alcoholic solvent and its cyclization to isopulegol have been also proposed to occur.

Citral hydrogenation at 333 K was carried out over the mono- and bimetallic catalysts after reduction at 673 K. The results of the test are summarized in Table 2. The slope of the linear region of the plots of conversion vs. time was used to determine the initial rates for each catalyst. It can be seen that the initial activities for the two monometallic Ru catalysts are similar. However, Fe/C presents negligible activity under our experimental condition. The selectivity for the unsaturated alcohols (geraniol and nerol) is the same for the two ruthenium catalysts (38 and 39%) and follows the same trend in the whole range of conversion (Fig. 3). Moreover, mainly one of the two unsaturated alcohols, geraniol, is produced by hydrogenation of the C=O bond. Similar selectivities to unsaturated alcohols have been found (38) for activated carbon-supported ruthenium catalysts with different metal particle sizes. However, these results, in a first approach, contrast with those previously reported by Gallezot and co-workers (9, 39). These authors found selectivities to the unsaturated alcohol in the hydrogenation of cinamaldehyde in liquid phase for group VIII metals supported on graphite that were higher than for those supported on activated

TABLE 2

Catalytic Properties in the Hydrogenation of Citral

Catalyst	Activity (μmol · g^{-1} · s^{-1})	S_{G+N}[a] (%)
Ru/C	1.12	39
RuFe/C	1.02	52
RuFe2/C	0.97	69
Fe/C	0	—
Ru/H	1.24	38
RuFe/H	1.07	66
RuFe2/H	0.41	73

[a] Selectivity to geraniol and nerol at 70% conversion.

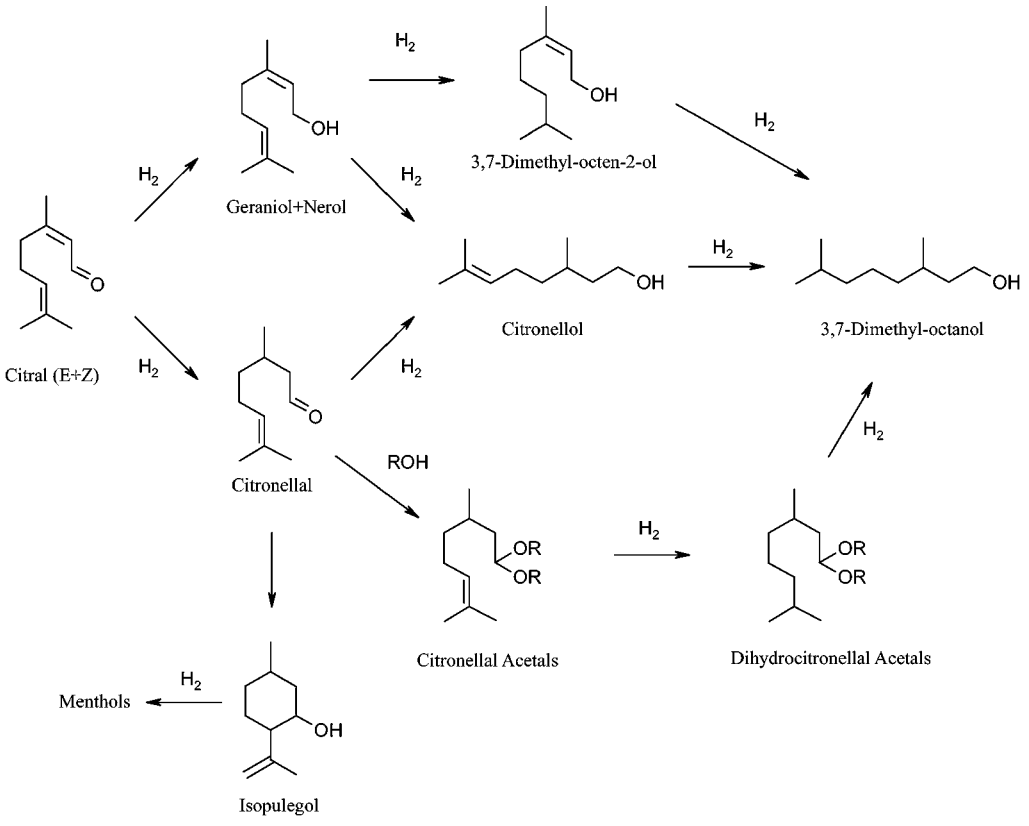

SCHEME 1

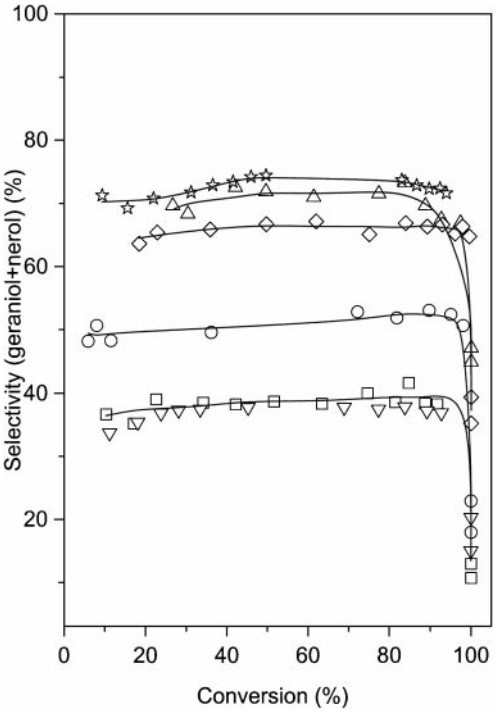

FIG. 3. Evolution of selectivity toward geranio + nerol with conversion in the citral hydrogenation at 333 K for (□) Ru/C, (○) RuFe/C, (△) RuFe2/C, (▽) Ru/H, (◇) RuFe/H, and (☆) RuFe2/H.

carbon, particularly for Pt and Ru. They attributed this fact to an electron transfer from the graphite to the metal particles grafted on edge planes that modify the mode of adsorption of the organic molecule. However, they use oxygen prefunctionalized graphite and charcoal supports to prepare the catalysts by ion exchange with metal ammine chloride precursors. These facts suggest that on one hand, the presence of oxygen functional groups at the surface of the graphite impedes the electron donor effect of the macroligand graphite, but on the other hand, it provides anchoring sites for the chloride anions. As has been earlier shown (8) for graphite-supported platinum and ruthenium catalysts, the presence of a small amount of residual chloride in the catalyst promotes the selective hydrogenation of α,β-unsaturated aldehydes toward unsaturated alcohols. The calorimetric experiments over Ru/C and Ru/H samples do not show changes in the differential heat of CO adsorption. From here, it can be inferred that the electron density of Ru particles in the catalyst supported on graphite is similar to that supported on activated carbon. So, modifications in selectivity to geraniol and nerol are not expected. In spite of the similarity in unsaturated alcohol selectivity, somewhat different behavior in the hydrogenation reaction was found for these two catalysts. Figure 4 shows the composition of the reaction mixture as a function of conversion

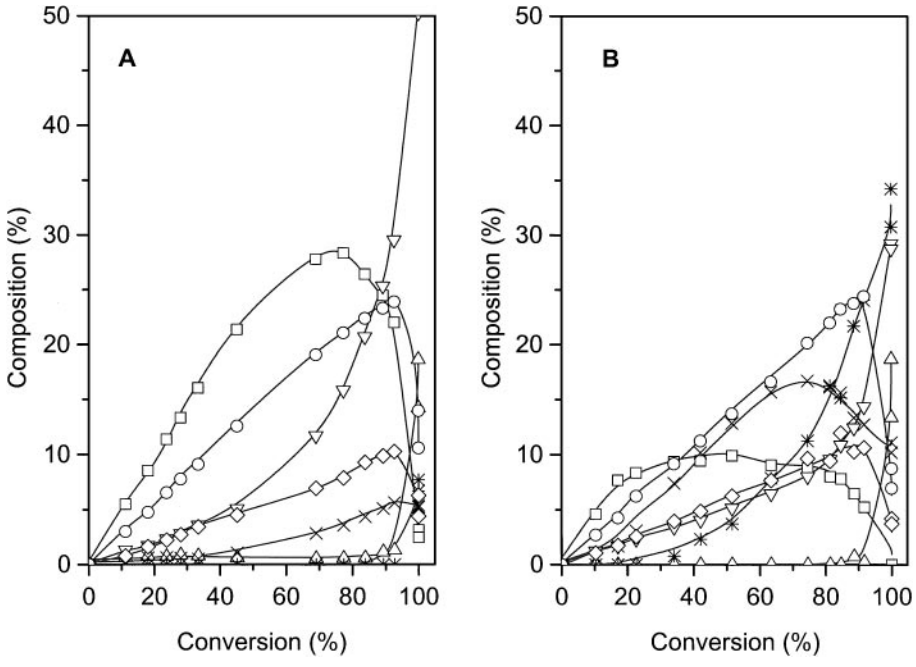

FIG. 4. Hydrogenation of citral at 333 K over Ru/H (A) and Ru/C (B). (□) Citronellal, (○) geraniol, (◇) nerol, (▽) citronellol, (△) 3,7-dimethyloctanol, (∗) other products, and (×) acetals of citronellal.

for Ru/C and Ru/H. In the first step of the reaction, Ru/H produces citronellal and unsaturated alcohols as the main products. A small amount of citronellol is also obtained. At higher reaction times, the consumption of the primary products by further hydrogenation to citronellol and finally to 3,7-dimethyloctanol is observed. The secondary reactions of citronellal, forming acetals and isopulegol, occur to a lesser extent, with the formation of the latter being almost inhibited. On Ru/C catalysts, acetals of citronellal were formed in the first stages of the reaction. Citronellal was obtained in a lower amount than on a Ru/H catalyst. The formation of acetals leads to the hydrogenation of the terminal C=C double bond, producing the acetals of dihydrocitronellal (included in other products), and subsequently less citronellol is obtained. These results agree with those previously reported for the hydrogenation of citral on supported ruthenium catalysts (40). Furthermore, isopulegol (included in other products) is formed on the Ru/C catalyst by cyclization of citronellal.

The reactions of isomerization of citronellal forming isopulegol and the reaction of citronellal with the solvent forming acetals have been associated with the existence of acid sites in the catalyst (39, 41, 42). It has been suggested that the catalyst is a bifunctional system, where isomerization occurs on the surface of the support and the hydrogenation of C=C and C=O bonds occurs on the metal particles (41). Carbon materials with clean surfaces do not present acid sites and therefore the occurrence of these reactions would be inhibited on these supports. However, as discussed above, although the original carbon materials used as support have clean surfaces, during impregnation with the oxidizing solution of the metal precursor, a certain number of surface oxygen groups were created. The TPD experiments have shown that the surface oxygen groups are mainly carboxyl groups, which confer acidic character to the carbon surface. Moreover, given that the proportion of active sites increases as the surface area of the carbon increases, the content of surface oxygen functional groups is higher in the activated carbon. Therefore, it can be understood that an activated carbon-supported ruthenium catalyst produces more reactions catalyzed by acid sites than does a Ru/H catalyst. These results agree with those reported by Milone *et al.* (41). They found a relationship between the chemical nature of the support and the product distribution of the citronellal hydrogenation.

The use of iron as a promoter in ruthenium catalysts supported on activated carbon and on graphite does not have a pronounced effect on initial activity except for RuFe2/H, which presents a marked decrease (Table 2). Concerning selectivity, we can see in Table 2 and Fig. 3 that the addition of iron favors the production of geraniol and nerol. The increase in selectivity to these compounds with increasing iron loading is much clearer for the samples supported on activated carbon than for those supported on high-surface-area graphite. For the former catalysts, selectivity increases from 39% for Ru/C to 52 and 69% for the 0.4 and 2.0 Fe/Ru ratios, respectively. In graphite-supported catalysts, selectivities obtained for the two iron loadings

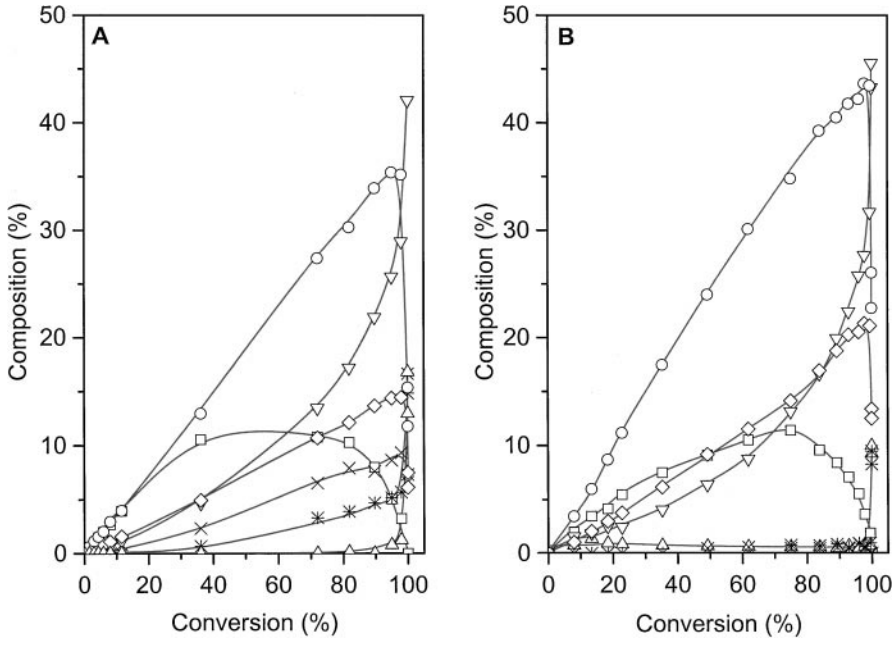

FIG. 5. Hydrogenation of citral at 333 K over RuFe/C (A) and RuFe/H (B). (□) Citronellal, (○) geraniol, (◇) nerol, (▽) citronellol, (△) 3,7-dimethyloctanol, (∗) other products, and (×) acetals of citronellal.

are 66 and 73%. The product distribution displayed for the bimetallic catalysts also changed with respect the monometallic counterpart. It is observed in Fig. 5A for RuFe/C that geraniol is the main product of the reaction and that the citronellal formed is subsequently hydrogenated to citronellol after 50% of citral conversion. Compared with the monometallic Ru/C catalyst, the increase in the initial citronellal selectivity is accompanied by a decrease in selectivities to acetal of citronellal and to other secondary products. That is, a mitigation in the acid site catalyzed reactions is observed. Selectivity to geraniol and nerol decreases after total conversion of citral due to its further hydrogenation to citronellol and to *cis*- and *trans*-3,7-dimethyl-octen-2-ol. Similar patterns were obtained for RuFe2/C, but the secondary reactions of citronellal were totally inhibited. The decrease in the acid site catalyzed reactions for RuFe/C and RuFe2/C catalysts correspond with a reduction in the surface population of oxygen groups on the samples, as seen in TPD experiments. In the case of the catalysts supported on graphite, both catalysts show comparable profiles and in Fig. 5B it is displayed for RuFe/H. Geraniol is the main product but citronellal was also detected. The most important fact is that the small amount of citronellal acetals detected with Ru/H is absent with both RuFe/H and RuFe2/H. The two isomers of 3,7-dimethyl-octen-2-ol were observed after the disappearance of citral. From the reduction of the secondary reactions catalyzed by acid sites over the bimetallic catalysts, a diminution in the surface oxygen group population of these catalysts can be inferred. This is explained by the less oxidizing character of the solution employed for the coimpregnation of the supports during the preparation procedure.

4. CONCLUSION

The increase in selectivity to unsaturated alcohols for the Ru–Fe catalysts is in line with that previously reported for supported group VIII metal catalysts promoted with a second element, particularly Sn and Fe. The enhancement of selectivity in hydrogenating the carbonyl group has been associated with the presence of polarity at the metal surface (3). And two mechanisms have been proposed for the promoting effect in the bimetallic catalysts: (i) The promoter acts as an electrophilic or Lewis site activating the C=O bond and favoring its adsorption and hydrogenation, or (ii) the promoter acts as electron-donor ligand, increasing the electron density of the active metal, which reduces the adsorption of the C=C bond and its hydrogenation. However, the mode of action and the state of the promoter added were not definitively known under working conditions and modern techniques were used to improve the catalyst characterization.

From the techniques applied in the present work to characterize the catalysts, the formation of Ru–Fe alloy can be inferred. It is clear from the TPR experiments that the two metals are in close interaction. The reduction of Fe is shifted to lower temperatures and it could be considered that the iron is present in a totally reduced state. Our calorimetric experiments have shown that the promoted catalysts supported on activated carbon and on graphite exhibit heats of

CO adsorption intermediate between the two monometallic extremes. As discussed above, this fact implies a Ru–Fe alloy formation.

The formation of an alloy and its role in the hydrogenation of unsaturated aldehydes has been a controversial issue. In the hydrogenation of citral with Rh–Sn catalysts supported on silica, and prepared using an organometallic route or by impregnation and oxidation-reduction activation, the alloy was almost unselective toward unsaturated alcohols and no electronic effects due to electron transfer from Sn to Rh were present (15, 18, 43). On the other hand, Claus (4) found the highest selectivity to crotylalcohol in the hydrogenation of crotonaldehyde over supported group VIII metal M–Sn/SiO_2 (M = Rh, Pt, or Ru) catalysts prepared using controlled surface reaction. The author considers that the $Rh^{\delta-} - Sn^{\delta+}$ bimetallic sites of the alloyed phase are the selective sites for the C=O hydrogenation (4). In the case of iron, Pt–Fe alloys over carbon prepared *ex situ* or by adding $FeCl_2$ to the solution have shown excellent values of selectivity in the hydrogenation of cinnamaldehyde (10, 44).

The catalytic results presented in this paper give additional support for evidence of the important role of alloyed phase in determining unsaturated alcohol selectivity. Thus, alloy particles of ruthenium with the more electropositive metal, iron, exhibit surface polarity, which is necessary for interacting with the oxygen atom of the carbonyl group of the α,β-unsaturated aldehyde. Therefore, mechanism (i), described above, is considered to account for the promoting effect of iron. So, the iron species in the alloy act as Lewis sites for the activation of the C=O bond, which is easily hydrogenated by addition of hydrogen chemisorbed on the nearby ruthenium species.

In conclusion, the Ru–Fe alloy supported on activated carbon and on graphite is very selective for the production of unsaturated alcohols (geraniol + nerol) by the selective hydrogenation of citral. This selectivity is independent of the carbonaceous support used, probably due to the presence of oxygen groups at the edges of the graphitic layers, which restrains the electron transfer from graphite to metallic particles. Moreover, the oxygen groups with acidic character created at the surface of the carbonaceous supports catalyze secondary reactions, whose extension is a function of their population.

ACKNOWLEDGMENTS

The financial support of the CICYT of Spain under project MAT-1999-1005 is acknowledged. One of the authors, P. W., thanks the Spanish Agency of International Cooperation for a scholarship grant.

REFERENCES

1. Mimoun, H., *Chimia* **50**, 620 (1996).
2. Bauer, K., and Garbe, D., "Common Fragance and Flavor Materials." VCH, Weinheim, 1985.
3. Gallezot, P., and Richard, D., *Catal. Rev.— Sci. Eng.* **40**, 81 (1998).
4. Claus, P., *Topics Catal.* **5**, 51 (1998).
5. Ponec, V., *Appl. Catal. A* **149**, 27 (1997).
6. Coloma, F., Sepúlveda-Escribano, A., Fierro, J. L. G., and Rodríguez-Reinoso, F., *Appl. Catal. A* **150**, 165 (1997).
7. Coloma, F., Narciso-Romero, J., Sepúlveda-Escribano, A., and Rodríguez-Reinoso, F., *Carbon* **36**, 1011 (1998).
8. Bachiller-Baeza, B., Guerrero-Ruiz, A., and Rodríguez-Ramos, I., *Appl. Catal. A* **192**, 289 (2000).
9. Giroir-Fendler, A., Richard, D., and Gallezot, P., *Stud. Surf. Sci. Catal.* **41**, 171 (1988).
10. Richard, D., Ockelford, J., Giroir-Fendler, A., and Gallezot, P., *Catal. Lett.* **3**, 53 (1989).
11. Galvagno, S., Donato, A., Neri, G., Pietropaolo, R., and Pietropaolo, D., *J. Mol. Catal.* **49**, 223 (1989).
12. Marinelli, T. B. L. W., Nabuurs, S., and Ponec, V., *J. Catal.* **151**, 431 (1995).
13. English, M., Ranade, V. S., and Lercher, J. A., *J. Mol. Catal. A* **121**, 69 (1997).
14. Coq, B., Figueras, F., Moreau, C., Moreau, P., and Warawdekar, M., *Catal. Lett.* **22**, 189 (1993).
15. Sordelli, L., Psaro, R., Vlaic, G., Cepparo, A., Recchia, S., Dossi, C., Fusi, A., and Zanoni, R., *J. Catal.* **182**, 186 (1999).
16. Nishiyama, S., Hara, T., Tsuruya, S., and Masai, M., *J. Phys. Chem. B* **103**, 4431 (1999).
17. Margitfalvi, J. L., Tompos, A., Kolosova, I., and Valyon, J., *J. Catal.* **174**, 246 (1998).
18. Coupé, J. N., Jordão, E., Fraga, M. A., and Mendes, M. J., *Appl. Catal. A* **199**, 45 (2000).
19. Sokolskii, D. V., Anisimova, N. V., Zharmagambetova, A. K., Mukhamedzhenova, S. G., and Edygenova, L. N., *React. Kinet. Catal. Lett.* **33**, 399 (1987).
20. Goupil, D., Fouilloux, P., and Maurel, R., *React. Kinet. Catal. Lett.* **35**, 185 (1987).
21. Guerrero-Ruiz, A., Badenes, P., and Rodríguez-Ramos, I., *Appl. Catal. A* **173**, 313 (1998).
22. Guerrero-Ruiz, A., Sepúlveda-Escribano, A., and Rodríguez-Ramos, I., *Appl. Catal. A* **120**, 71 (1994).
23. Badenes, P., Daza, L., Rodríguez-Ramos, I., and Guerrero-Ruiz, A., *Stud. Surf. Sci. Catal.* **112**, 241 (1997).
24. Illán-Gomez, M. J., Raymundo-Piñero, E., García-García, A., Linares-Solano, A., and Salinas-Martínez de Lecea, C., *Appl. Catal. B* **20**, 267 (1999).
25. Guerrero-Ruiz, A., Sepúlveda-Escribano, A., and Rodríguez-Ramos, I., *Appl. Catal. A* **81**, 81 (1992).
26. Jung, H.-J., Vannice, M. A., Mulay, L. N., Stainfield, R. M., and Delgass, W. N., *J. Catal.* **76**, 208 (1982).
27. Burch, R., and Hayes, M. J., *J. Catal.* **165**, 249 (1997).
28. Guerrero-Ruiz, A., *Appl. Catal.* **55**, 21 (1989).
29. Guerrero-Ruiz, A., Bachiller-Baeza, B., and Rodríguez-Ramos, I., *Appl. Catal. A* **173**, 231 (1998).
30. Radovic, L. R., and Rodríguez-Reinoso, F., *in* "Chemistry and Physics of Carbon" (P. A. Thrower, Ed.), Vol. 25, p. 276. Dekker, New York, 1997.
31. Rodríguez-Reinoso, F., Guerrero-Ruiz, A., Moreno-Castilla, C., Rodriguez-Ramos, I., and López-Gonzalez, J. D., *Appl. Catal.* **23**, 299 (1986).
32. Bein, T., and Jacobs, P. A., *J. Chem. Soc., Faraday Trans. 1* **79**, 1819 (1983).
33. Schüneman, V., Treviño, H., Lei, G. D., Tomczak, D. C., Sachtler, W. M. H., Fgash, K., and Dumesic, J. A., *J. Catal.* **153**, 144 (1995).
34. Toyoshima, I., and Somorjai, G. A., *Catal. Rev.—Sci. Eng.* **19**, 105 (1979).

35. Topsoe, H., Topsoe, N., Bohlbro, H., and Vannice, J. A., *Stud. Surf. Sci. Catal.* **7**, 247 (1981).
36. Ott, G. L., Fleisch, T., and Delgass, W. N., *J. Catal.* **60**, 394 (1979).
37. Kaminsky, M., Yoon, K. J., Geoffroy, G. L., and Vannice, M. A., *J. Catal.* **91**, 338 (1985).
38. Galvagno, S., Milone, C., Donato, A., Neri, G., and Pietropaolo, R., *Catal. Lett.* **18**, 349 (1993).
39. Gallezot, P., and Richard, D., *Sci. Technol.* **47**, 28 (1994).
40. Neri, G., Mercadante, L., Donato, A., Visco, A. M., and Galvagno, S., *Catal. Lett.* **29**, 379 (1994).
41. Milone, C., Gangemi, C., Ingoglia, R., Neri, G., and Galvagno, S., *Appl. Catal. A* **184**, 89 (1999).
42. Yadav, G. D., and Nair, J. J., *J. Chem. Soc., Chem. Commun.* 2369 (1998).
43. Didillon, B., El Mansour, A., Candy, J. P., Bournonville, J. P., and Bassel J. M., *in* "Heterogeneous Catalysis and Fine Chemicals II" (M. Guisnet, J. Barrault, C. Bouchoule, D. Duprez, G. Pérot, R. Maurel, and C. Montassier, Eds.), p. 137. Elsevier, Amsterdam, 1991.
44. Goupil, D., Fouilloux, P., and Maurel, R., *React. Kinet. Catal. Lett.* **35**, 185 (1987).